Acta Materialia **48**(9), 2349–2362 (2000)

A study of aluminium foam formation - kinetics and microstructure

I. Duarte*, J. Banhart

Fraunhofer-Institute for Advanced Materials,

Wiener Str. 12, 28359 Bremen, Germany

Abstract

Aluminium foams were produced by applying the powder compact melting method, i.e. by mixing metal powders and powdered gas-releasing blowing agents and pressing them to a foamable precursor material after this. The resulting precursor was then foamed by heating it up to above its melting point inside an „expandometer“, which allowed for a control of volume and temperature throughout the entire process. The present studies comprise the effects of the aluminium alloy composition (AlSi7 and 6061), some of the pressing parameters of the foamable precursor material, the foaming temperature and the heating rate during foaming on the expansion behaviour of the foam. Moreover, the morphological and microstructural evolution of metal foams is investigated.

Kurzfassung

Aluminiumschäume wurden durch Aufschäumen von Pulverpreßlingen hergestellt. Dazu wurde eine Mischung bestehend aus Metallpulvern und einem gasabspaltenden Treibmittel in einem ersten Schritt zu einem aufschäumbaren, dichten Vormaterial verpreßt. Dieses Vormaterial wurde dann durch Erwärmung auf eine Temperatur oberhalb seines Schmelzpunktes aufgeschäumt. Das Schäumen fand in einem „Expandometer“ statt, das die Messung von Schaumvolumen und -temperatur während des ganzen Prozesses erlaubt. Untersucht wurde der Einfluß der Legierungszusammensetzung (AlSi7 oder 6061), einiger Preßparameter des Vormaterials, der Schäumtemperatur sowie der Heizrate auf das Expansionsverhalten der Schäume. Außerdem wird die Entwicklung der Porenstruktur des Schaumes und der Mikrostruktur der Zellwände charakterisiert.

Keywords:	1. powder processing	2. image analysis, optical microscopy
	3. aluminium, foam	4. kinetics, stability

* Now at Instituto Nacional de Engenharia e Tecnologia Industrial, Estrada do Paço de Lumiar, 1649-038, Lisboa, Portugal

1 Introduction

Cellular metals can be produced by a variety of different methods [**1**]. Among these, metal foaming methods are especially attractive because they allow for manufacturing fairly inexpensive closed-cell materials with attractive mechanical properties. By „foaming“ one usually means releasing gas in a liquid, ensuring that the gas bubbles do not escape and by finally stabilising the liquid foam by cooling [**2**].

A manufacturing method for producing closed-cell metal foams from metal powders was developed some years ago [**3-5**]. The process consists of mixing metal powder and a powdered blowing agent and compacting the mix to a dense semi-finished product (called „foamable precursor material“) by hot pressing, extrusion, powder rolling or other methods. In a final step the foamable precursor material is expanded by heating it up to above its melting point. This transfers the metal into a semi-liquid viscous state and simultaneously makes the blowing agent decompose thus releasing gas and creating a highly porous structure.

Metal foams have been characterised thoroughly with respect to their morphology, their mechanical properties and to other properties important for potential applications [**6,7**]. However, there is still only very little work (see e.g. Ref.’s **8** to **10**) on how the foam emerges from the liquid, how it changes with time and what mechanisms are responsible for its formation. The present paper intends to help closing this gap.

Monitoring the foaming process of liquid metals is much more difficult that doing the same e.g. with aqueous foams. Many of the observation techniques used for such foams cannot be applied owing to the specific properties of liquid metals: they are hot, opaque, very reactive with oxygen and have a high electrical conductivity. This rules out optical or resistometric methods which are often used for investigating aqueous foams [**11,12**]. One can distinguish two kinds of possible techniques for investigating the foaming process of metals: ex-situ measurements and in-situ measurements. In the first case a foam is produced by heating up a precursor thus initiating bubble growth and foam formation. After a given time the foaming process is interrupted by cooling and the resulting solid foam is characterised. By varying the time between the beginning of the experiment and the interruption of foaming one obtains a series of samples which reflect the various stages of foam evolution. The disadvantage of this approach is that it takes a long time to carry out such investigations and that the results bear a certain inaccuracy originating in statistical variations between the single experiments. Even if the starting materials for the individual foaming experiments were produced in the same way, each foaming experiment would turn out slightly differently due to

effects such as accidental agglomerates of the blowing agent, structural defects in the precursor material, impurities, etc. Therefore, in-situ methods for characterising metal foams are preferred in which a parameter characterising the foam is measured during the evolution of one single sample. Unfortunately, such measurements are very difficult to carry out and at the moment only the most simple parameter, the foam volume, can be measured in-situ.

In the present work the evolution of foam volume, pore morphology (shape and size), and foam microstructure will be studied. Only the volume is measured in-situ, while pore morphologies and microstructures are characterised on samples that were quenched from different evolution stages of a growing or collapsing foam.

2 Preparation of materials

Two aluminium alloys were used which have gained importance in metal foaming. The wrought alloy 6061 is used whenever high strength and a good corrosion resistance are desired. The casting alloy AlSi7 is applied in composite structures of foam and aluminium sheets or tubes because it has a low melting point and a good foamability. Two foamable aluminium alloys - 6061 or AlSi7 - each containing 0.6 wt.% TiH_2 (titanium hydride) were produced either by extrusion (for 6061) or by hot pressing (for AlSi7). In both cases metal and blowing agent powders were mixed in appropriate quantities in a tumbling mixer. Pre-alloyed air-atomised 6061 powders (main alloying elements: 0.4-0.8% Si, 0.8-1.2% Mg, <0.7% Fe) were used for the first alloy, whereas AlSi7 alloys (which are similar to the casting alloys A356 or A444) were obtained by blending elementary aluminium (also air-atomised) and silicon powders. Table 1 lists some of the powder properties. The first two columns contain data given by the powder manufacturer, whereas the powder size spectrum was measured with a Coulter particle size analyser, the oxide content with a Leco TC436 oxygen/nitrogen determinator by the authors.

For extrusion 50 kg of the powder mix were first compacted to cylindrical slugs of 70 to 80% theoretical density by cold isostatic pressing (CIP) [**13**]. Although this step is not absolutely necessary, it helps to facilitate handling of the slugs and also in avoiding de-mixing and contamination of the powders. The slugs were then pre-heated to 360°C and extruded to rectangular bars of 160x20mm^2 cross-section in a second step in which a horizontal 25 MN direct extrusion machine was used. Tablets of 9 mm thickness and 31 mm diameter were machined out of the extruded bars for the foaming tests.

Hot pressing consisted of axially densifying the powder mixture in a cylindrical die in two steps (see **Table 2**): first the powders were filled into the die and placed into a furnace which was pre-heated to the pressing temperature **T.** The mixture was then pressed at a constant pre-pressing pressure $\mathbf{p_1}$ during which the temperature of the initially cold powder and die rose to the furnace temperature T. After a given period $\mathbf{t_1}$ the pressure was increased to $\mathbf{p_2}$ and the actual hot pressing took place for a given time $\mathbf{t_2}$. The function of the pre-pressing step is to avoid the powders from uncontrolled oxidation during heating to the hot pressing temperature. The pressed samples were 10 mm thick and 32 mm in diameter so that they could easily be machined to the dimensions needed for the expandometer (9 x 31 mm).

Figure 1 shows optical images of the microstructure of both foamable precursor materials after pressing. One sees that the compacted powders are virtually pore free in both cases. Light grey TiH_2 particles can be seen in the metal matrix of both alloys. The darker angular shaped silicon particles are only observed in the metallic matrix of the AlSi7 alloy. Due to the difficulty to distinguish TiH_2 and silicon particles on optical micrographs, EDX will be used in the further work to help in identifying these particles.

3 Experimental Procedure

The tests were performed by foaming the precursor tablets inside a so-called „laser expandometer“ which is explained in **Figure 2**. The metal foam is created inside a small cylindrical steel mould (diameter: 32 mm, height: 70 mm) which is open only at the top. The mould is located in the centre of a quartz glass tube (1400 mm long, 140 mm diameter) where it is held by a sample support made of stainless steel. The heat source is a folding furnace with a cylindrical chamber of 150 mm diameter and 650 mm height. The furnace is guided by rails and can be slid around the foaming tube within a few seconds. For future applications the glass tube can be operated under variable pressures and atmospheres and is therefore connected to a pump and gas source. However, in the present study all foaming took place at normal atmosphere.

Two foaming procedures were applied: in the first mode the furnace was pre-heated to the desired temperature without the foaming tube being in it. After this, the hot furnace was closed around the glass tube of the expandometer causing an immediate rise of the temperature at the sample site. This created the fastest possible temperature rise. Alternatively, the cold furnace was first closed around the glass tube and after that the furnace

was heated from room temperature to the desired temperature at a given rate. This way tests at low heating rates could be performed.

For the foaming tests a piece of foamable precursor material was placed inside the steel mould and was then heated. The laser sensor that was attached to the top of the quartz tube constantly measured the position of the upper side of the sample through the open top side of the mould thus allowing to monitor the rise of the emerging foam. In addition, the temperature of the expanding sample and the surroundings of the mould were constantly measured with thermocouples. Both the thermocouples and the laser sensor were connected to a computer via an A/D interface. The data was recorded and analysed with a standard acquisition programme which allows for a direct visualisation of the data already during the experiment. The measurement of the volume V of the expanding melt together with the sample temperature T_s generated a pair of functions V(t) and $T_s(t)$ which characterise the expansion kinetics. The measured data can be displayed as a pair of functions - $[V(t),T_s(t)]$ - or as one function $V(T_s)$ with the time as an implicit parameter.

The calibration of the laser expandometer was carried out at room temperature using various samples of a known height. Empty runs without any sample - i.e. measuring the distance between laser sensor and sample support - were then performed with the furnace at various pre-set temperatures to obtain the expansion characteristics of the empty instrument, originating mainly in the thermal expansion of the sample support and the quartz tube. The data was parametrised and stored. The actual measurements on aluminium foam samples could then be corrected automatically for the expansion of the instrument using this correction data.

The acquired data was smoothed in order to eliminate noise coming from the laser sensor. This noise is caused by thermal fluctuations in the atmosphere inside the glass tube during foaming. Smoothing with a time constant in the order of a few seconds removed much of this noise. Moreover, the laser expandometer sometimes showed strong fluctuations in the heating phase before foaming and, occasionally, even negative volume readings (see e.g. Figure 4). These are not real expansion effects but artefacts having their origin in the strong turbulences in the furnace which mainly occur when it is heated up from room temperature. In later stages of the experiment the turbulences diminish because the temperature distribution in the furnace becomes more uniform and stationary and therefore these unwanted effects disappear.

The laser sensor could measure distances with an accuracy of 0.1 % and a resolution of 0.02%. In the present application, however, this accuracy was not achieved because of the

effects already mentioned and is not even necessary because of the nature of the foam surface which is uneven, curved and in constant change due to expanding and coalescing bubbles. Therefore no meaningful interpretation of effects on a length scale of less than about one millimetre can be given.

4 Results and discussion

4.1 Reproducibility tests

As foam growth is a statistical process, two foaming experiments will never yield exactly the same result even if the initial conditions were „identical“, i.e. the same within the limits of experimental accuracy. Accidental agglomerates of blowing agent particles in the foamable precursor or unpredictable heat transfer between the heat source and the foamable precursor samples are possible sources for irreproducibilities. Moreover, the experimental set-up might contain elements which limit reproducibility of foaming experiments, such as, e.g., friction effects between foam and mould which are hardly reproducible. In order to get an idea of how reproducible foaming tests can be, five samples of 6061 precursor material which were machined out of the same extruded rod were foamed at the same nominal furnace temperature. **Figure 3** shows the resulting temperature and volume curves for these samples as a function of time. What is obvious is that there is a scatter on the time scale of the different expansion curves. One reason for this is that the data recording programme was started only after a certain delay time after the furnace had been closed around the foaming tube to allow the vibrations caused by the furnace movement to be damped out. Therefore the sample temperature at t=0 is higher than room temperature in all cases. This influence together with the possibly different heat transfer rate between mould and sample - which depends on whether the sample touches the mould only in some points or with significant parts of its surface - causes the observed shift of the various V(t) curves against each other. Maximum expansion occurs between 620 and 700 seconds after the start of data acquisition. Nevertheless, all samples show almost the same maximum expansion of about 50 mm. If one eliminates the time by plotting V(T) (see right hand side of Figure 3) the foaming behaviour of all alloys appears almost identical.

We conclude that foaming tests can be carried out in a reproducible way. However, differences in maximum foaming height of less than 5 mm seem to be insignificant. In practical tests we always carried out a minimum of two tests on identical samples and compared the results. If there seemed to be too much difference between the two results (e.g. significantly more than difference between the samples in Figure 3), further tests were carried

out. However, if the curves were similar in this sense an average curve was calculated. All volume expansion curves shown in the next sections are averages of at least two individual measurements.

4.2 Comparison with previous results

In previous studies the foaming process of aluminium alloys was characterised by means of an apparatus which used a ceramic movable piston instead of a laser [**14,15**]. The expanding foam displaced the piston and generated the volume expansion function V(t) this way. The aim of a first test was to compare expansion curves given by this (old) expandometer – called „mechanical expandometer“ and the one using the laser sensor – called „laser expandometer“. For this various foamable precursor samples as described in Sec. 2 were used [**10**].

The results can be summarised as follows: both data sets show the same stages of foam formation, namely: a) below the solidus temperature of the aluminium alloy, the expansion is small; b) as the solidus temperature of the aluminium alloy is reached, it starts to soften and expands slowly as a consequence of the decomposition of TiH_2 to H_2 gas and Ti; c) as the temperature increases, the expansion rate increases rapidly until the maximum expansion is reached; d) finally, the blowing agent is exhausted and no longer releases hydrogen and the foam starts to collapse. However, there are also some differences between the curves obtained by the two instruments, namely: a) the mechanical expandometer shows a lower maximum expansion due to the weight of the piston (9g) and effects counteracting expansion originating in friction between the piston, the emerging foam and the confining steel tube. Moreover, the laser measures the position of the centre of the expanding foam. As the foam expands without any restriction in the vertical direction, the surface of the foam is usually vaulted and the highest point of the foam generates the distance reading. Values given by the laser expandometer therefore tend to be slightly too high (approximately 2 mm); b) in the collapse regime the mechanical expandometer yields constant volume readings because the piston is blocked soon after collapse has begun.

From the comparison of the two instruments one can conclude that the laser sensor is a more sensitive tool to measure the expansion during the entire foaming process than the mechanical expandometer, because it does not disturb the foam during its growth and collapse.

4.3 Influence of compaction conditions

In order to evaluate the effect of some of the compaction parameters on the kinetics of the foaming process, samples of foamable precursor material were prepared under different conditions and characterised in the laser expandometer. As the conditions in the extrusion process could not be varied easily because a full-size industrial extrusion machine was used and batches of usually more than 100 kg have to be produced each time, the parameter study was carried out only with hot pressing which allows for the production of small batches and therefore for varying a larger number of different parameters. Foamable AlSi7 precursor tablets of the required size were pressed as described in Sec. 2 for various pressing parameters (see also **Table 2**). After pressing foaming tests were carried out using a pre-heated furnace at 750°C.

Figure 4 shows expansion curves of samples which were pressed at different hot pressing temperatures T ranging from 200°C to 550°C with constant pressing times t_1 and t_2. **Figure 5** shows expansion curves of samples which were hot pressed at different pre-pressing and hot pressing times t_1 and t_2 but at a constant hot pressing temperature of **450°C**. The pressures p_1 and p_2 were kept constant in all the tests.

It is obvious that the hot pressing temperature is a critical parameter for the foaming behaviour (**Figure 4**). The highest expansions are reached for hot pressing temperatures between 400°C and 450ºC. For higher and lower temperatures the maximum expansion is lower and in the extreme case, for 200°C and 550°C, virtually no foaming can be observed any more. The reason for this is that for low compaction temperatures only insufficient densification with a high degree of residual open porosity is achieved, corresponding to a low density of the foamable precursor material (see values given below **Figure 4**). Thus hydrogen gas can escape from the melting precursor through the system of interconnected channels and does not create and inflate bubbles. About 1% residual porosity appears to be the tolerable limit for this particular alloy system. In the other extreme, too high compaction temperatures also lead to lower maximum expansions because hydrogen is lost already during hot compaction. This loss is almost complete for a compaction temperature of 550°C. Thermoanalysis of free TiH_2 powder shows that decomposition begins at 380°C and continues up to 570°C. However, these results are valid only for free powders and depend also on the heating rates applied in the tests and on the environmental atmosphere. The optimum hot pressing temperature around 400°C to 450°C is therefore near the initial decomposition temperature of free TiH_2 powder, but this does not harm the TiH_2 embedded in the gas-tight embodiment of the metallic matrix of the foamable precursor material.

It is interesting to note that the samples compacted at temperatures T≤450°C show a

transient expansion peak after which the foam quickly relaxes by a few millimetres to reach an almost constant volume (marked in Figure 4). This peak could be a consequence of excess hydrogen in the precursor material which is weakly bound and is released in an early stage of foaming. The excess hydrogen could possibly cause a too quick inflation of pores and a corresponding partial collapse of some thin-walled membranes. The sample pressed at 500°C does not show this behaviour and reaches a stable state without showing the transient peak. This is understandable since compaction of the powder mix at 500°C is just sufficient to drive out this excess hydrogen while this temperature is still too low to remove all the blowing gas. This, however, happens at 550°C compaction temperature. From the measurements one can therefore conclude that the blowing agent content of 0.6 wt.% - usually used in the industrial production of foamable precursor material - is unnecessarily high and should be slightly reduced. As titanium hydride is quite expensive, this would help to reduce costs.

Figure 5 demonstrates that the compaction time is a fairly uncritical parameter for the hot pressing temperature and pressure chosen. The expansion curves are all quite similar the remaining differences being within the range of normal statistical fluctuations.

4.4 Influence of foaming conditions

4.4.1 Furnace temperature

Foamable precursor samples of AlSi7 and 6061 alloys as described in Sec. 2 were used for studying the influence of the furnace temperature on foaming kinetics. The foaming tests were performed using a pre-heated furnace which was slid around the glass tube containing the sample for the test. The nominal furnace temperature was varied between 600°C and 800°C. **Figure 6** shows the influence of temperature on the foaming behaviour of the two aluminium alloys studied. The curves are labelled with the nominal furnace temperature which, however, does not coincide with the sample temperature at any time. Heat losses through the ends of the cylindrical furnace which are closed by the glass tube only are the reason that even after a long test time the sample temperature is lower than the nominal furnace temperature by 35 to 50°C. In the further discussion we shall therefore also refer to the final temperature in the sample. In Figure 6 the solidus and liquidus temperatures of the two alloys are shown as horizontal dotted lines. The measured values (AlSi7: 577°C/620°C; 6061: 610°C/664°C) deviate slightly from what one expects from the literature [**16,17**] - in particular the measured liquidus temperature is about 10°C too high - but this does not change the conclusions.

It is evident that the foaming process depends sensitively on the foaming temperature chosen. If the final sample temperature is below the solidus temperature of the alloy (T_1 for AlSi7, T_2 for 6061) there is not very much more effect than a slight solid state expansion. If the final temperature lies in the solidus/liquidus interval (T_2 for AlSi7, T_4 for 6061) foam formation can be observed but especially for 6061 it is limited to quite low expansions around 100%. The viscosity of the semi-molten material is still quite high in this temperature and surface oxidation leads to an additional resistance towards bubble inflation counteracting the internal gas pressure built up by the decomposing blowing agent. Increasingly higher temperatures reduce viscosity and promote gas production so that higher and higher volume expansions can be observed. Beside reducing viscosity high furnace temperatures naturally also lead to high heating rates. This can be advantageous for obtaining high volume expansions as will be shown in the following section. The volume expansion seems to almost saturate out for AlSi7 at 750°C, whereas the maximum of foam expansion for the 6061 alloy is presumably at temperatures above the maximum temperature at which the furnace can be operated (800°C) as can be seen from **Figure 7** which displays the maximum expansion as a function of nominal furnace temperature $T_{furnace}$, final temperature in the sample T_{final} and the temperature in the moment of maximum expansion $T_{max.exp.}$. The difference between nominal furnace temperature and the final sample temperature has already been explained. Comparing the two temperatures T_{final} and $T_{max.exp}$ one can see that they are almost identical for low furnace temperatures, i.e. the temperature does not rise any more after the maximum of expansion has been reached, whereas for high furnace temperatures the sample temperature continues to increase after maximum expansion and therefore $T_{final}>T_{max.exp}$. The latter situation seems to be a prerequisite for obtaining high expansion rates: one has to ensure a high heat flux into the sample up to maximum expansion by providing a furnace at a sufficiently high temperature.

The curves for AlSi7 in **Figure 6** show the same initial foaming peak which was already explained in the previous section. It only occurs for the higher furnace temperatures. If the furnace is operated at or below 700°C nominal temperature the excess hydrogen can escape without creating an additional expansion effect during the comparatively slow heating phase.

4.4.2. Influence of heating rate

Different furnace temperatures lead to different heating rates and influence the foaming process this way. In order to evaluate the influence of the heating rate independently

of temperature, foaming tests were carried out at 800°C at different heating rates. For this the cold furnace was put around the glass tube containing the samples before it was then heated up at the given rate. **Figure 8** shows three expansion curves obtained this way. The fourth curve corresponds to the highest heating rate which was obtained by using a pre-heated furnace at 800°C as described in the previous sections.

Clearly, higher heating rates lead to an earlier expansion of the foamable precursor material because the melting temperature is reached at an earlier time. Beside this rather obvious difference the three expansion curves for the highest heating rates are very similar. Only a significantly lower heating rate leads to a change of the expansion characteristics, namely a lower maximum expansion. The main possible reasons for the drop in foamability for low heating rates are: i) gas losses due to the decomposition of titanium hydride during the slow transition through the temperature range from above 500°C where decomposition is rapid (see Sec. 4.3) and the temperature where foaming begins; ii) oxidation which could produce non-metallic layers on the surface of the precursor sample and even inside the sample in regions accessible to air by direct channels. Such oxide layers could contain alumina, magnesia or mixed oxides (6061 alloys contain magnesium) which remain solid throughout the foaming process and therefore mechanically hinder expansion.

4.5 Evolution of pore morphology during foaming

In order to observe the evolution of pore morphology of 6061 and AlSi7 aluminium alloys during foaming, a series of tests was performed in a pre-heated furnace at 800°C and 750°C, respectively. These temperatures were derived from **Figure 6** and ensure a good foamability of the two alloys. For each sample of the series the foaming process was stopped in a different stage of evolution by removing the furnace from the quartz tube at a given time derived from the known volume expansion curves for the respective alloys (given in principle in Figure 6, but re-measured for this purpose). After this the metal foam specimens were cooled to room temperature quickly. The expansion curve V(t) and the temperature T(t) were recorded throughout the experiment.

Figure 9a and **10a** show typical expansion curves for the two alloys. The points marked with capital letters **A**–**K** and **A'-K'** indicate the different foaming stages that were prepared (to be more precise, the stages at which the furnace was removed from the glass tube. As there is a certain after-expansion the samples were in a slightly more expanded state after cooling to room temperature than indicated in Figures 9a and 10a after final cooling). In **Figure 9b** and **10b** the corresponding micrographs of the various foaming stages are shown

(the foamable precursor material is identified by „**P**“). As can be seen from the micrographs, both aluminium alloys show the same foaming stages, namely: a) initiation and evolution of porosity: pores elongated perpendicular to the compaction direction (which was from top to bottom) are formed (phases **A** and **A'**); b) pore growth: the pores are inflated by the evolving hydrogen and are increasingly rounded off as the foam expands (**B-G** and **B'-G'**). The initial anisotropy starts to vanish until only a slight asphericity remains. Moreover, initially round pores are deformed to more polyhedral pores as the level of porosity increases and no more space can be filled by spherical pores; c) collapse: after maximum expansion no more hydrogen gas is released and the foam begins to decay. This decay leads to foams with large and irregular pores, collapsed and oxidised pores especially at the top of the sample and to a solid metal layer at the bottom (see **H-K** and **H'-K'**).

It is obvious that foam growth is neither isotropic nor uniform in both alloys investigated. The anisotropy has its origin in the texture created in the powder compact during solidification. In hot pressed tablets always oblate pores are formed and the following rise of the foam is along the original axis of pressing, whereas round extruded rods (not used in the present study) would rather expand in radial direction. Non-uniformities in the emerging foam are probably caused by local agglomerates of blowing agent or structural defects in the precursor material created by insufficient densification, impurities, or local oxidation. As the decomposition of TiH_2 already starts rather early at about 380ºC, i.e. in the solid state, tiny voids in the precursor material are formed preferably near such structural defects and lead to the formation of heterogeneous pore morphologies in the subsequent foam expansion.

Foam owe their collapse to two mechanisms, *drainage* and *coalescence*. Drainage is the flow of molten metal from the cell walls into the cell edges (driven mainly by surface tension) and through cell edges downwards driven by gravity (see **H-K** in **Figure 9b** and **H'-K'** in **Figure 10b**). A thick layer of metal at the bottom of the samples is the result of this process. Coalescence occurs whenever two cells merge to one large one. It is thought that cell rupture is the reason for such processes but no definite investigations have been carried out yet. It seems that metal membranes are not as stretchable as, e.g., the membranes in soap foams and rupture as soon as their thickness has fallen below a certain limit.

The collapse behaviour of the two aluminium alloys is quite different. After maximum expansion the AlSi7 foam does not loose its shape so much as the 6061 foam. In the 6061 foam a thick layer of metal at the bottom is formed. Moreover, the upper surface of the 6061 samples show more decay and the vaulted shape disappears. In contrast, the AlSi7 foam

samples remain vaulted and maintain a more regular cellular structure throughout the entire test.

4.6 Evolution of microstructure during foaming

The microstructural evolution of the cell walls of AlSi7 foam during the foaming process was investigated by analysing the samples obtained by interrupting the foaming process in various stages which were described in the previous section. AlSi7 was chosen because more easily visible microstructural changes were expected in this material initially containing two different elementary powders. One question to be answered is how alloying of the elementary particles takes place and whether it is acceptable to use elementary powder mixes instead of the more expensive pre-alloyed powders to make a given alloy foam. First of all the precursor material is revisited in **Figure 11**. SEM micrographs and an EDX-distribution map of silicon and titanium were obtained. The SEM picture shows that although silicon particles of many different sizes are present the distribution is quite uniform. The EDX element maps for silicon confirms this observation. Moreover, it is important that the titanium (hydride) is also distributed quite uniformly.

Figure 12 shows the pore morphology, the microstructure and the silicon distribution in different foaming stages. The stages are marked according to Figure 10a. Foaming times and sample temperatures are given in the column at the right.

Foaming stage **A'** still shows individual angular silicon particles (middle column, dark grey) embedded in the aluminium matrix (white). Quite some pores (dark) can bee seen already in this stage. As the temperature is slightly below the eutectic line (577°C) this is understandable. No liquid phase is present and interdiffusion times are long. Just 77 seconds later in phase **B'** the situation has completely changed. The temperature is now 16°C above the eutectic temperature and the metals have formed an alloy. The microstructure shows the typical α-Al grains (white) surrounded by a dark silicon-rich phase. Many of the grain boundaries are probably identical to former powder particles as can be seen from the grain near the cell wall marked with 'X'. Although the powders are densified during hot pressing, the oxide layers covering each individual powder particle survive even in the semi-liquid state. The silicon-rich melt accumulates preferably near such oxides thus forming the observed grain boundaries. Another 77 seconds later in phase **D'** we see a largely expanded foam at 634°C. The grains have grown slightly as compared to phase **B'** and the silicon distribution map (right column) shows that silicon is spreading and forms increasingly larger Al-Si regions. This tendency continues for the further stages of foaming. After 50 minutes

both the micrograph and the silicon distribution map shows the typical microstructure of a cast Al-Si alloy with light α-Al grains and heterogeneous Al-Si regions with their characteristic dark silicon needles [16].

5 Summary

The foaming kinetics of aluminium alloys foams produced by applying the powder compact melting route are determined by a complex interplay of several mechanisms which occur during the process. Foaming is strongly governed by temperature effects: the expansion curve depends on the hot pressing temperature for obtaining the foamable precursor material and the heating parameters during foaming. Hot pressing the powders at 400-450°C and using a furnace pre-heated to temperatures well above the liquidus temperatures of the alloys investigated was found to yield the best results. Making alloy foams from elementary powders is unproblematic at least for Al-Si alloys because alloying of the elements takes place quickly during foaming and a homogeneous microstructure is obtained after a short time. This is an important conclusion under the viewpoint of cost efficiency.

Acknowledgements

The work was supported by the European Union (Marie Curie Training Programme ERB-BRMA-CT98-5103) and Deutsche Forschungsgemeinschaft (Programme SPP-1075, Ba 1170/3-1).

References

[1] Banhart J., *Manufacture, characterisation and application of cellular metals and metal foams*, Prog. Mater. Sci., accepted for publication (1999)

[2] Banhart J., *Foam metal: the recipe*, Europhysics news **30**, 17 (1999)

[3] Baumeister J., *Verfahren zur Herstellung poröser Metallkörper*, German Patent 40 18 360 (1990), see also US Patent 5,151,246 (1992)

[4] Banhart J., Baumeister J., Weber M., *Powder metallurgical technology for the production of metal foam*, Proceedings of the European Conference on Advanced PM Materials, Birmingham 23.-25.10.1995 (1995), p. 201

[5] Banhart J., Baumeister J., *Deformation characteristics of metal foams*, J. Mater. Sci. **33**, 1431 (1998)

[6] Banhart J., Ashby M.F., Fleck N.A., *Metal foams and porous metal structures*, MIT-Verlag Bremen (1999)

[7] Ashby M.F., Evans A.G., Hutchinson J.W., Fleck N.A., *Metal foams: a design guide*, in press

[8] F. Simancík, Minariková N., Culák S., Kovacík J., *Effect of foaming parameters on the pore size*, in Ref. [6], p. 105

[9] Körner C., Singer R.F., *Numerical simulation of foam formation and evolution with modified cellular automata*, in Ref. [6], p. 91

[10] Duarte I., Weigand P. Banhart J., *Foaming kinetics of aluminium alloys*, in Ref. [6], p. 97

[11] Weaire D., Hutzler S., *The physics of foams*, Oxford University Press (1999)

[12] Weaire D., Banhart J., *Foams and films*, MIT-Verlag Bremen (1999)

[13] Baumgärtner F., Gers H., *Industrialisation of P/M foaming process*, in Ref. [6], p. 73

[14] Banhart, P. Weigand P., *Powder metallurgical process for the production of metallic foams*, in Proc. Fraunhofer USA Symposium Metallic Foams, Ed. J. Banhart and H. Eifert, MIT-Verlag Bremen, p. 13, (1998)

[15] Weigand P., *Untersuchungen der Einflußfaktoren auf die pulvermetallurgische Herstellung von Aluminiumschäumen*, MIT-Verlag, Bremen (1999)

[16] Davis J.R. (Editor), *Aluminium and aluminium alloys*, ASM Handbook, ASM Information Society, Materials Park OH (USA) (1993)

[17] Massalski T.B., *Binary alloy phase diagrams*, ASM Information Society, Materials Park OH (USA) (1986)

Tables

Table 1: Some properties of the powders used. D_p means that p% of the particles are larger than the value given.

	Specifications by the powder supplier		measured powder properties				
Powders	purity [%]	size [μm]	D_{10} [μm]	D_{50} [μm]	D_{90} [μm]	mean diameter [μm]	oxygen content [%]
Al	99.7	< 160	128	57	17	67	0.7
Si	n. spec.	<100	91	30	4.4	48	0.5
6061 alloy	99.5	60-400	250	116	59	140	1.1
TiH_2	99	< 63	41	15	2.9	22	n.det.

Table 2: Hot pressing parameters for cylindical 32 mm die

step	temperature	time	pressure
pre-pressing	20°C $\rightarrow$ **T** (variable)	$\mathbf{t_1}$ (variable)	$\mathbf{p_1}$ = 60 kN
final pressing	**T** (variable)	$\mathbf{t_2}$ (variable)	$\mathbf{p_2}$ = 90 kN

Figure Captions

Figure 1: Foamable 6061 (left) and AlSi7 (right) precursor material containing 0.6 wt.% TiH_2.

Figure 2: Schematic drawing of the apparatus used for the foaming tests (not to scale).

Figure 3: Reproducibility tests on five 6061 samples foamed at 800°C. Left: time-resolved expansion and temperature, right: expansion vs. temperature.

Figure 4: Expansion curves of AlSi7 samples prepared at different hot pressing temperatures. Other parameters as given in Table 2. Absolute and relative densities of the hot pressed precursor samples are given (theoretical density of fully dense alloy = 2.68 g/cm^3).

Figure 5: Expansion curves of AlSi7 samples prepared with different pre-heating (t_1) and hot pressing times (t_2). The hot pressing temperature was 450°C in all cases.

Figure 6: Expansion (E) and temperature (T) curves of AlSi7 and 6061 alloys foamed at different nominal furnace temperatures (600°C-800°C, values given in the legend). Solidus and liquidus temperatures of the two alloys are given as horizontal dotted lines.

Figure 7: Maximum foam expansions of AlSi7 and 6061 alloys given as a function of various temperatures ($T_{furnace}$ = nominal furnace temperature, T_{final} = final temperature in the samples after 50 minutes of foaming, $T_{max.exp}$ = temperature in the sample in the moment of maximum expansion).

Figure 8: Foam expansion curves of 6061 alloys for different heating rates at 800°C nominal furnace temperature.

Figure 9: Expansion curve (a) and morphology in different foaming stages (b) for 6061 alloys using a pre-heated furnace at 800°C.

Figure 10: Expansion curve (a) and morphology in different foaming stages (b) for AlSi7 alloys using a pre-heated furnace at 750°C.

Figure 11: Large picture: SEM image of foamable AlSi7 precursor material (0.6 wt.% TiH_2). Aluminium matrix (dark grey), silicon particles (light grey) and TiH_2 particles (white) can be seen. The white frame shows the area for which EDX element distribution maps are shown for Si and Ti (small pictures).

Figure 12: Morphology (left column), optical micrographs (middle) and EDX silicon distribution (right column) of AlSi7 foams in different stages of expansion (not the same region of the sample shown in different columns). Letters denote the stage of expansion in which the furnace was removed from the expandometer tube according to Figure 10a, the times and temperatures refer to that particular moment. Note that due to the after-expansion

after this the foams shown on the photographs are more expanded than one would expect from the locations indicated in Figure 10a. Times are given in hh:mm:ss.

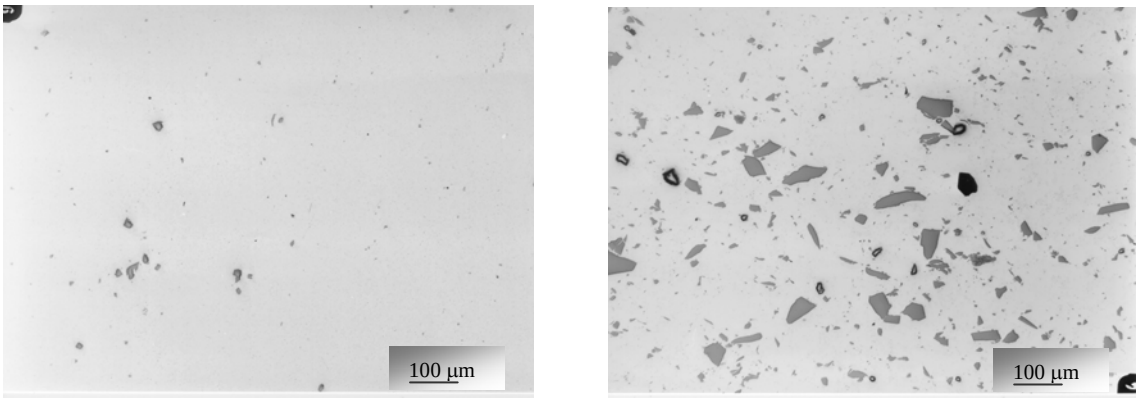

Figure 1: Foamable 6061 (left) and AlSi7 (right) precursor material containing 0.6 wt.% TiH_2.

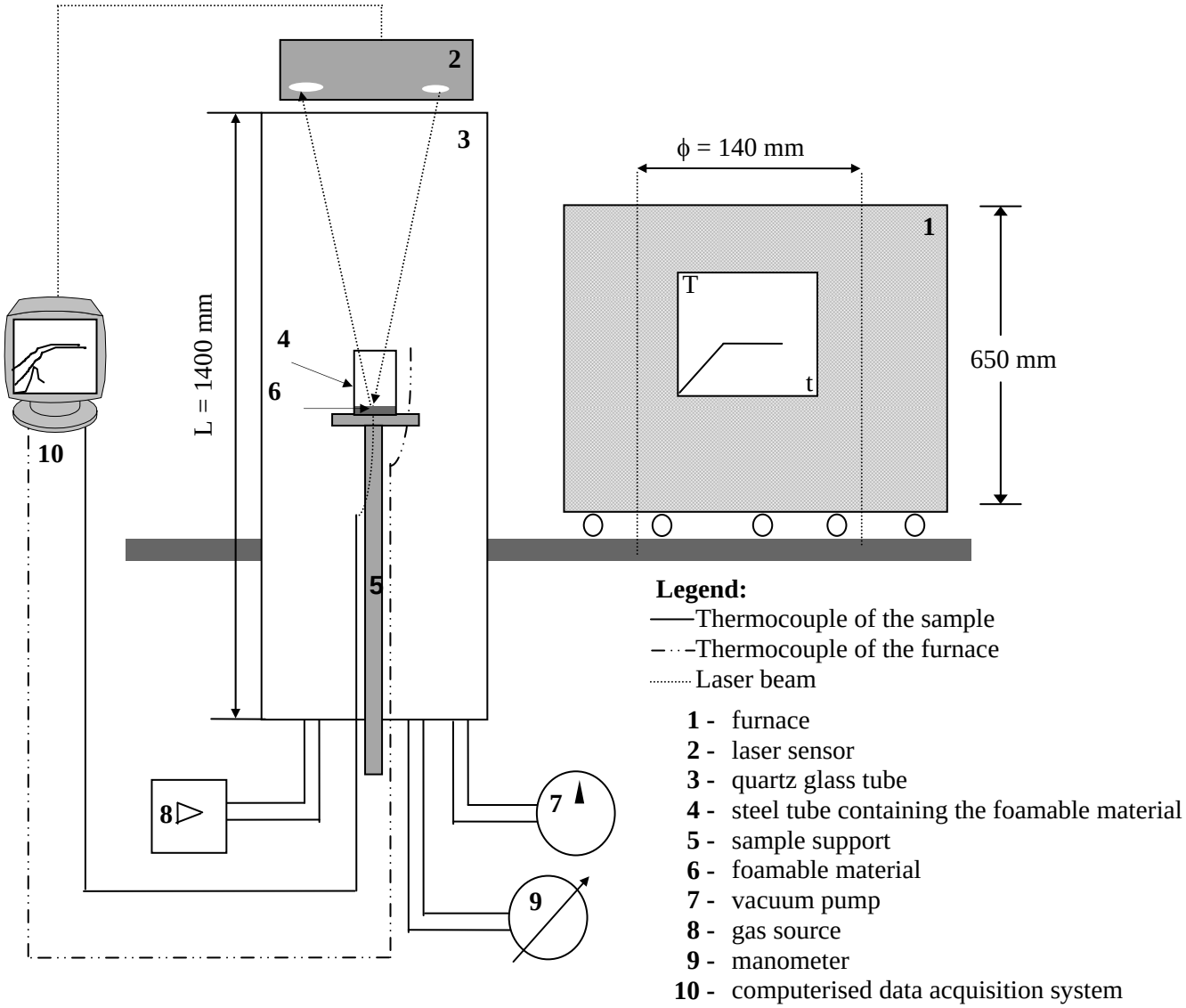

Figure 2: Schematic drawing of the apparatus used for the foaming tests (not to scale).

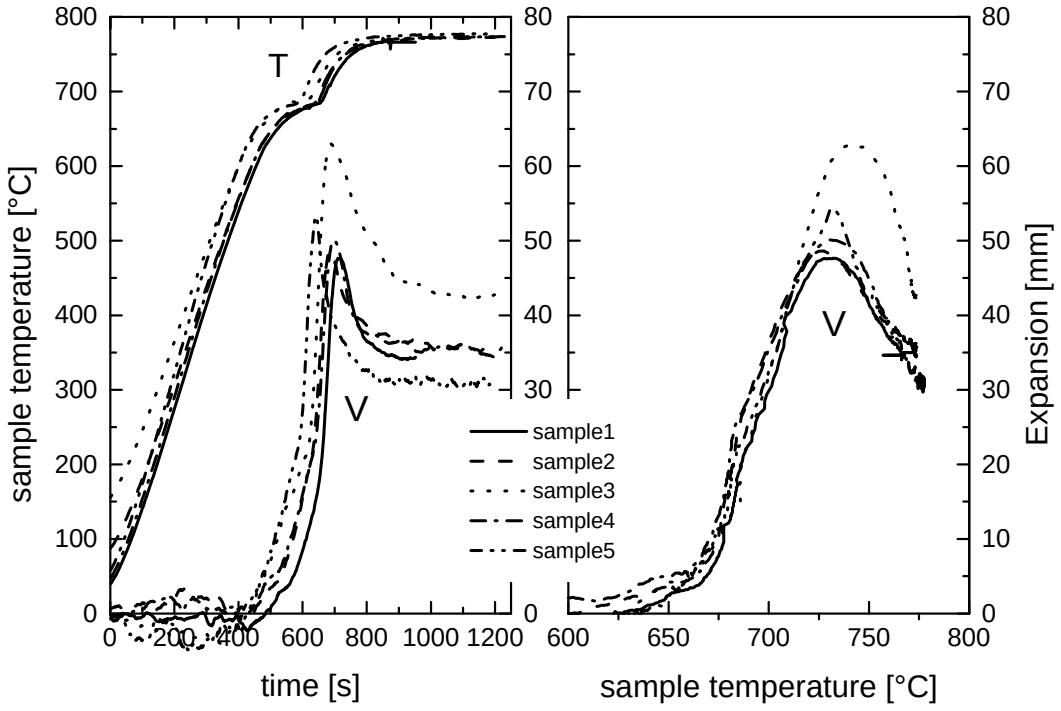

Figure 3: Reproducibility tests on five 6061 samples foamed at 800°C. Left: time-resolved expansion and temperature, right: expansion vs. temperature.

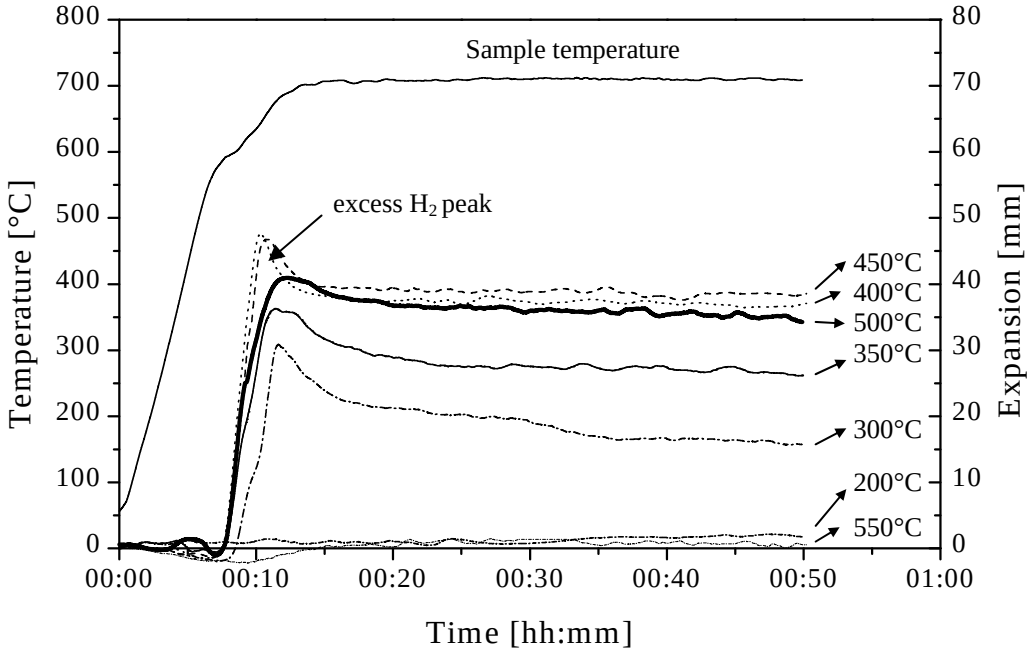

$T_{hot\ pressing}$ [°C]	200	300	350	400	450	500	550
$\rho_{average}$ [g/cm^3]	2.46	2.58	2.61	2.65	2.66	2.66	2.68
$\rho_{average}$ [%]	91.79	96.27	97.39	98.98	99.25	99.25	≈100

Figure 4: Expansion curves of AlSi7 samples prepared at different hot pressing temperatures. Other parameters as given in Table 2. Absolute and relative densities of the hot pressed precursor samples are given (theoretical density of fully dense alloy = 2.68 g/cm^3).

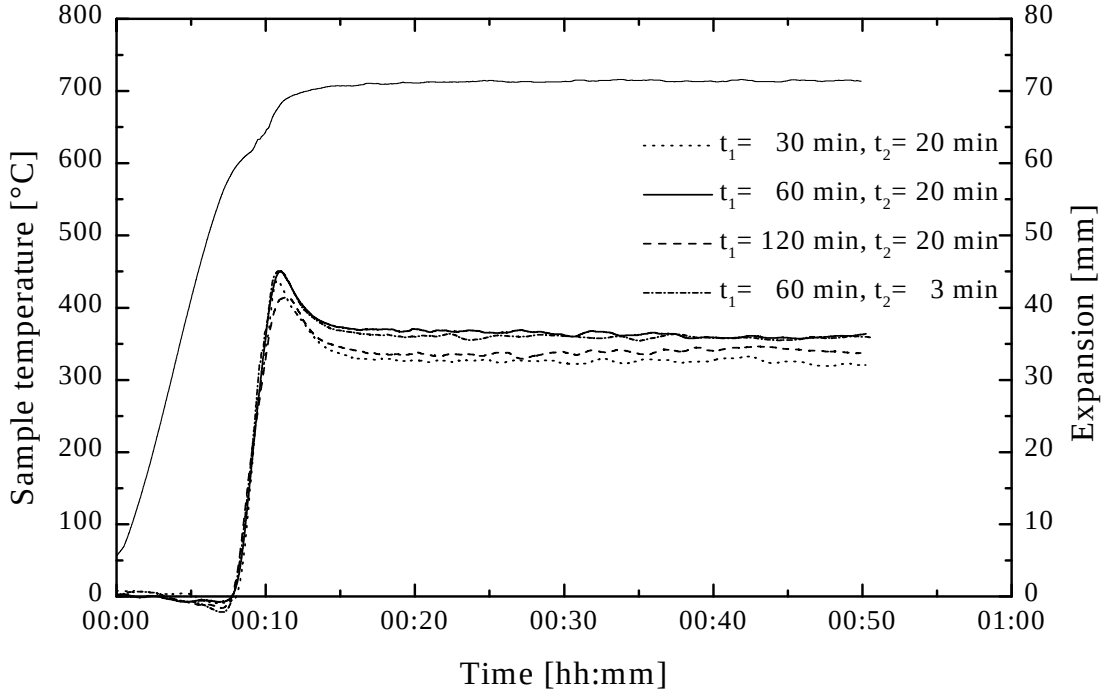

Figure 5: Expansion curves of AlSi7 samples prepared with different pre-heating (t_1) and hot pressing times (t_2). The hot pressing temperature was 450°C in all cases.

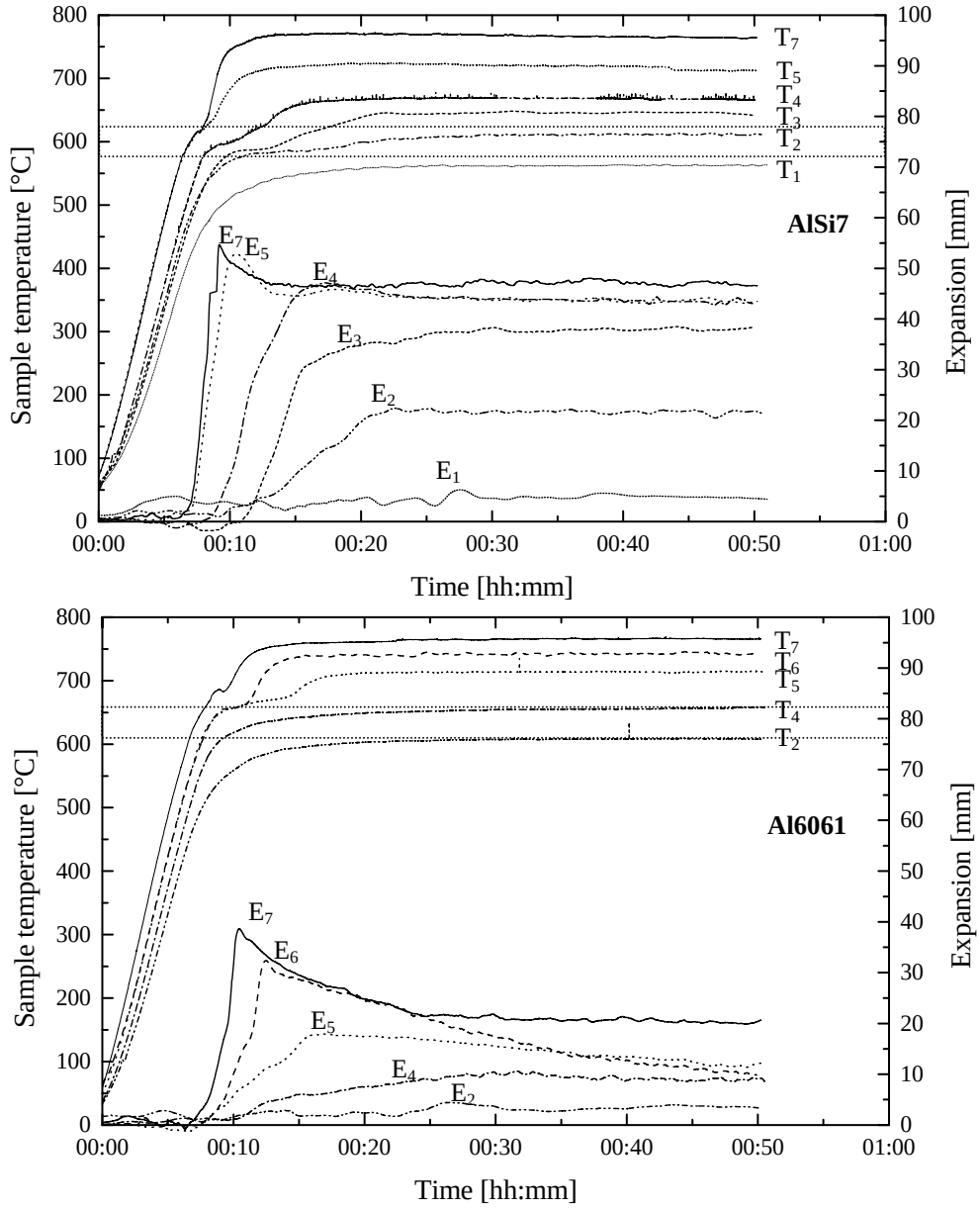

Legend:

$T_{furnace}$ [°C]	600	650	675	700	750	775	800
E curve	E_1	E_2	E_3	E_4	E_5	E_6	E_7
T curve	T_1	T_2	T_3	T_4	T_5	T_6	T_7

Figure 6: Expansion (E) and temperature (T) curves of AlSi7 and 6061 alloys foamed at different nominal furnace temperatures (600°C-800°C, values given in the legend). Solidus and liquidus temperatures of the two alloys are given as horizontal dotted lines.

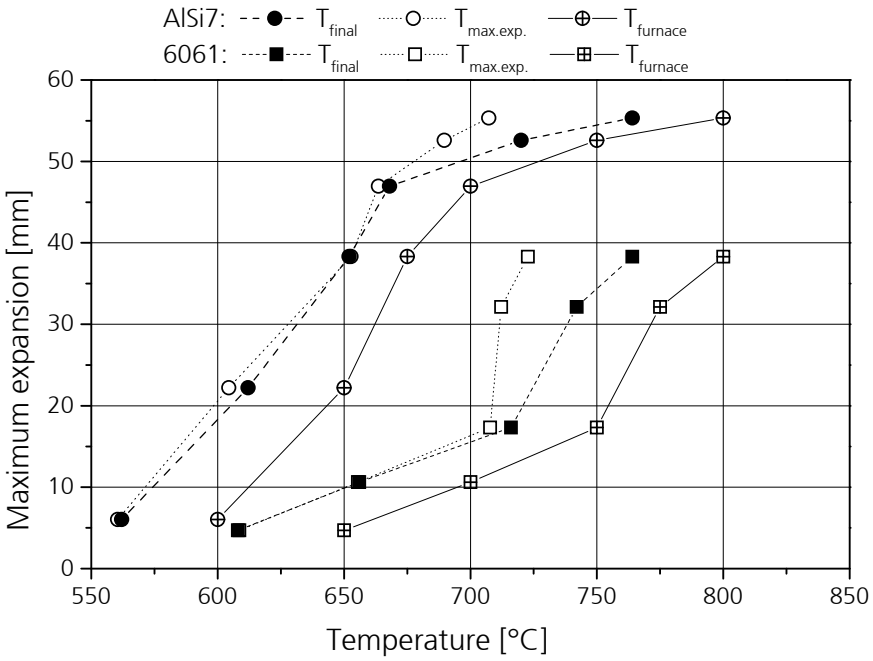

Figure 7: Maximum foam expansions of AlSi7 and 6061 alloys given as a function of various temperatures ($T_{furnace}$ = nominal furnace temperature, T_{final} = final temperature in the samples after 50 minutes of foaming, $T_{max.exp}$ = temperature in the sample in the moment of maximum expansion).

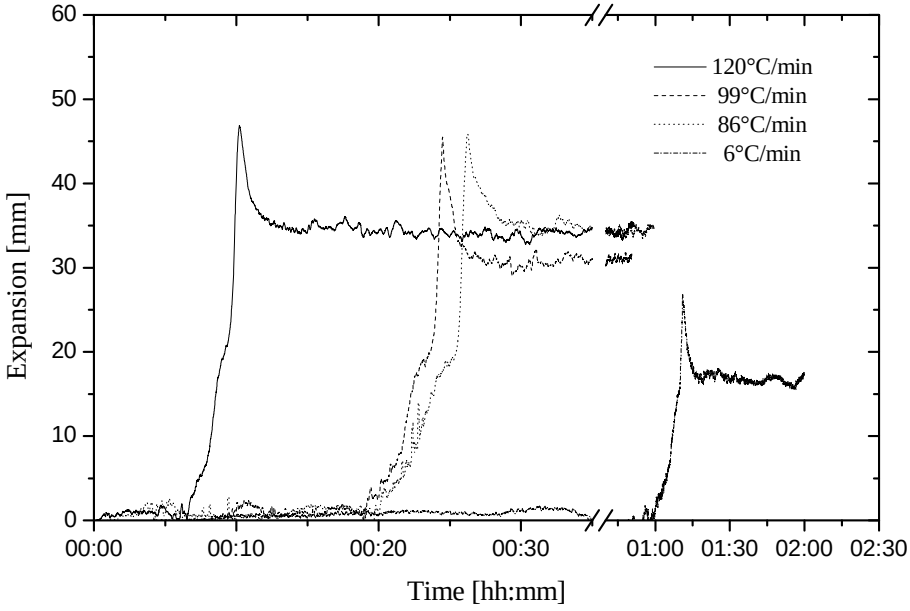

Figure 8: Foam expansion curves of 6061 alloys for different heating rates at 800°C nominal furnace temperature.

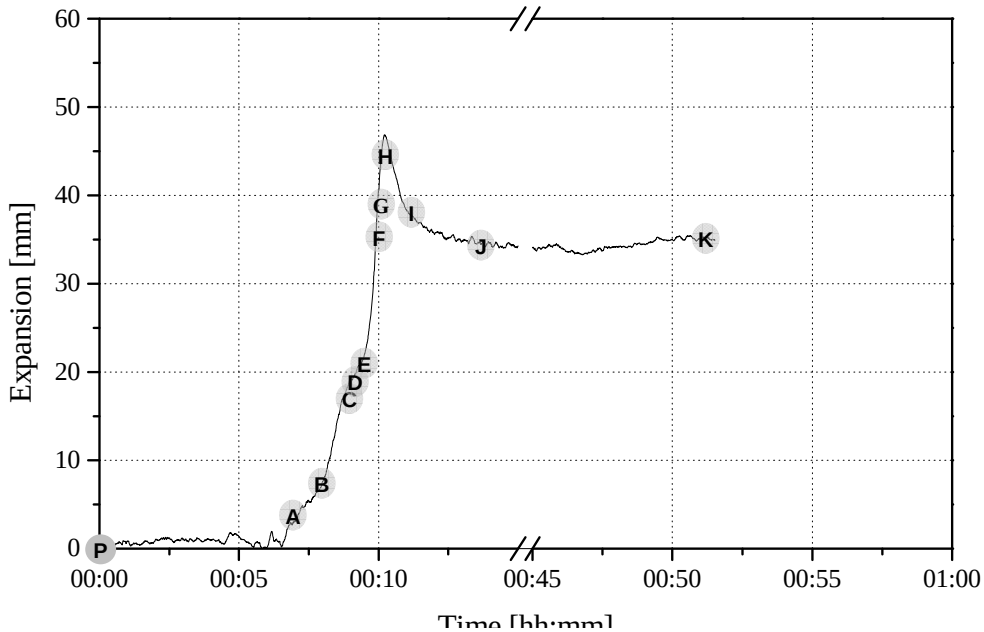

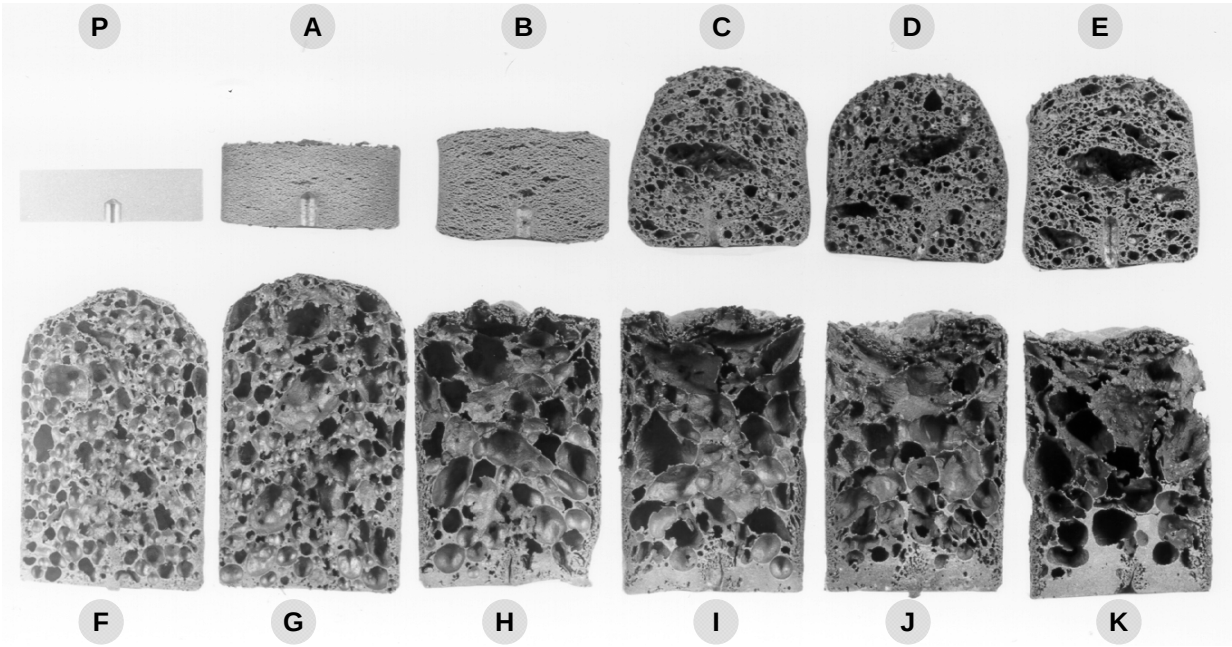

Figure 9: Expansion curve (a) and morphology in different foaming stages (b) for 6061 alloys using a pre-heated furnace at 800°C.

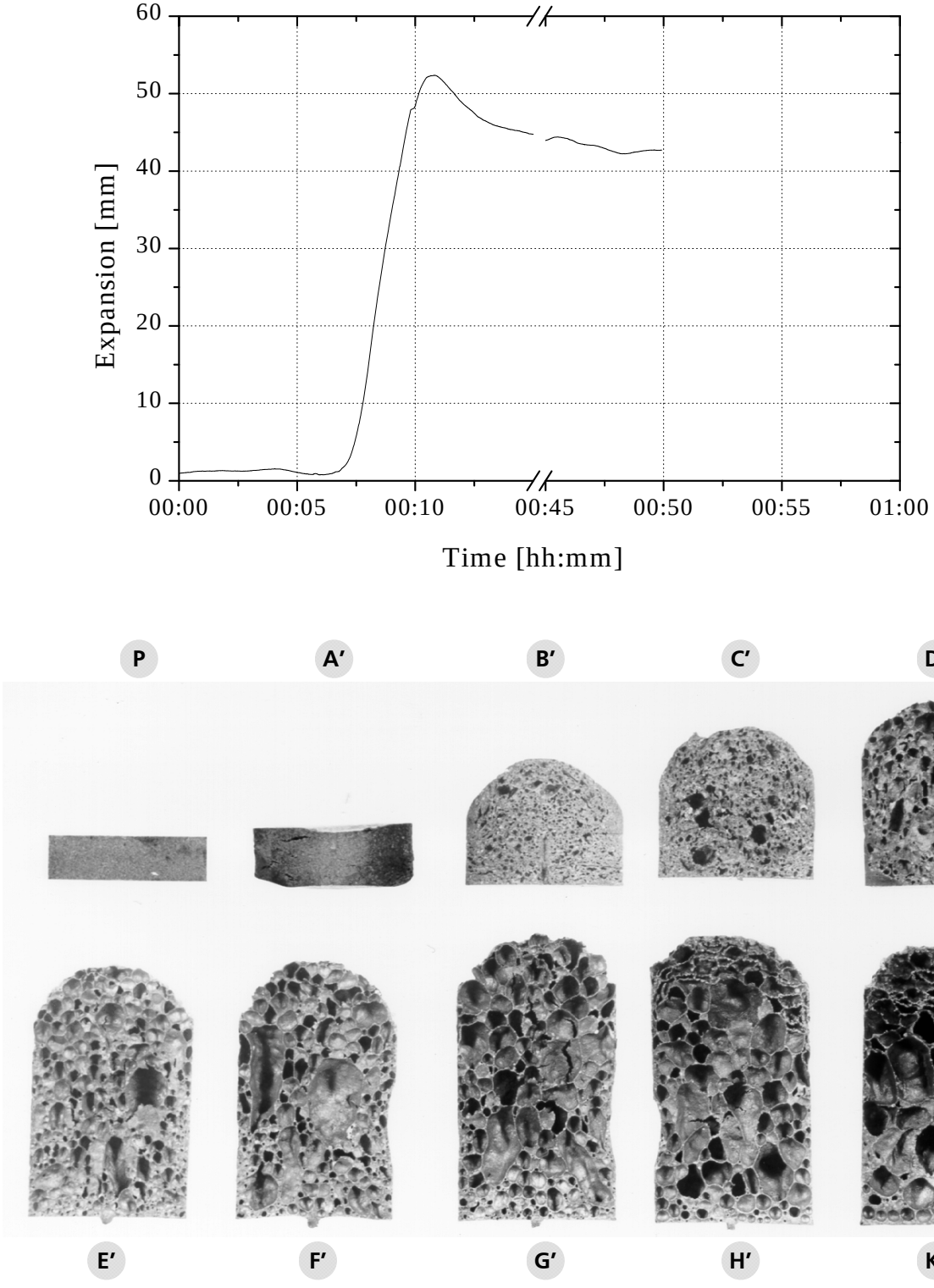

Figure 10: Expansion curve (a) and morphology in different foaming stages (b) for AlSi7 alloys using a pre-heated furnace at 750°C.

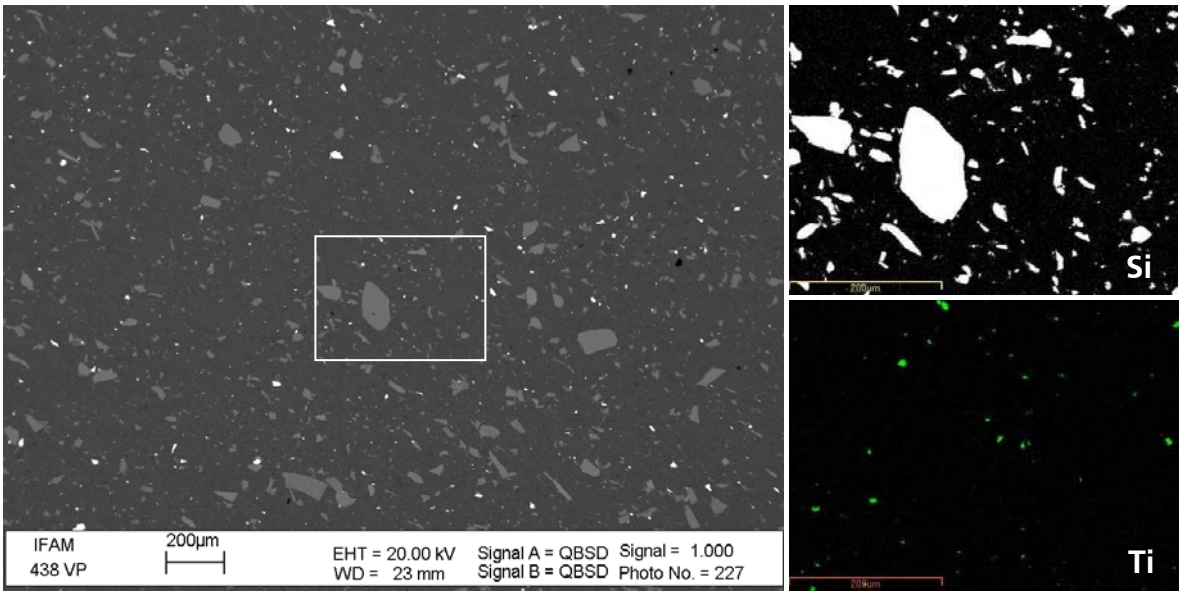

Figure 11: Large picture: SEM image of foamable AlSi7 precursor material (0.6 wt.% TiH_2). Aluminium matrix (dark gray), silicon particles (light gray) and TiH_2 particles (white) can be seen. The white frame shows the area for which EDX element distribution maps are shown for Si and Ti (small pictures).